Anomaly in the K-S(0)Sigma(+) photoproduction cross section off the proton at the K* threshold

Ewald, R.; Bantes, B.; Bartholomy, O.; Bayadilov, D.; Beck, R.; Beloglazov, Y. A.; Brinkmann, K. -T.; Crede, V.; Dutz, H.; Elsner, D.

Published in:
Physics Letters B

DOI:
10.1016/j.physletb.2012.05.066

Physics Letters B 713 (2012) 180–185

Contents lists available at SciVerse ScienceDirect

Physics Letters B

www.elsevier.com/locate/physletb

Anomaly in the $K^0_S\Sigma^+$ photoproduction cross section off the proton at the K^* threshold

CBELSA/TAPS Collaboration

R. Ewald [a,1], B. Bantes [a], O. Bartholomy [b], D. Bayadilov [b,c], R. Beck [b], Y.A. Beloglazov [c], K.-T. Brinkmann [b], V. Crede [b,d], H. Dutz [a], D. Elsner [a], K. Fornet-Ponse [a], F. Frommberger [a], Ch. Funke [b], A.B. Gridnev [c], E. Gutz [b], W. Hillert [a], J. Hannappel [a], P. Hoffmeister [b], I. Jaegle [e], O. Jahn [a], T. Jude [a], J. Junkersfeld [b], H. Kalinowsky [b], S. Kammer [a,1], V. Kleber [a,2], Frank Klein [a], Friedrich Klein [a], E. Klempt [b], B. Krusche [e], M. Lang [b], H. Löhner [f], I.V. Lopatin [c], D. Menze [a], T. Mertens [e], J.G. Messchendorp [f], V. Metag [g], M. Nanova [g], D. Novinski [b,c], R. Novotny [g], M. Ostrick [a,3], L. Pant [g,4], H. van Pee [b], A. Roy [g,5], S. Schadmand [g,6], C. Schmidt [b], H. Schmieden [a,*], B. Schoch [a], S. Shende [f], V. Sokhoyan [b], A. Süle [a], V.V. Sumachev [c], T. Szczepanek [b], U. Thoma [b], D. Trnka [g], R. Varma [g,5], D. Walther [b], Ch. Wendel [b]

[a] *Physikalisches Institut, Rheinische Friedrich-Wilhelms-Universität Bonn, Germany*
[b] *Helmholtz-Institut für Strahlen- und Kernphysik, Rheinische Friedrich-Wilhelms-Universität Bonn, Germany*
[c] *Petersburg Nuclear Physics Institute, Gatchina, Russia*
[d] *Department of Physics, Florida State University, Tallahassee, FL, USA*
[e] *Department of Physics and Astronomy, University of Basel, Switzerland*
[f] *Kernfysisch Versneller Instituut, Groningen, The Netherlands*
[g] *II. Physikalisches Institut, Universität Gießen, Germany*

ARTICLE INFO

Article history:
Received 28 December 2011
Received in revised form 28 May 2012
Accepted 31 May 2012
Available online 5 June 2012
Editor: D.F. Geesaman

Keywords:
Meson photoproduction
Strangeness
Cross section
Meson–baryon interaction
Dynamically generated resonance

ABSTRACT

The $\gamma + p \to K^0 + \Sigma^+$ photoproduction reaction is investigated in the energy region from threshold to $E_\gamma = 2250$ MeV. The differential cross section exhibits increasing forward-peaking with energy, but only up to the K^* threshold. Beyond, it suddenly returns to a flat distribution with the forward cross section dropping by a factor of four. In the total cross section a pronounced structure is observed between the $K^*\Lambda$ and $K^*\Sigma$ thresholds.

1. Introduction

The CBELSA/TAPS experiment at the electron stretcher accelerator ELSA [1] of Bonn University is investigating the excitation spectrum of the nucleon. Despite the impressive progress of ab initio lattice calculations of the spectrum of ground state baryon masses [2], excited states still prove challenging. Some features of resonances are successfully described by quark potential models, e.g. magnetic moments and electromagnetic couplings [3–5], others remain difficult to understand, e.g. the parity ordering of the lowest lying nucleon excitations $N(1440)P_{11}$ and $N(1535)S_{11}$. This

* Corresponding author.
E-mail address: schmieden@physik.uni-bonn.de (H. Schmieden).
[1] Now at DLR, Cologne, Germany.
[2] Now at German Research School for Simulation Sciences, Jülich, Germany.
[3] Present address: Institut für Kernphysik, Universität Mainz, Germany.
[4] On leave from Nucl. Phys. Division, BARC, Mumbai, India.
[5] On leave from Department of Physics, IIT, Mumbai, India.
[6] Present address: Institut für Kernphysik and Jülich Center for Hadron Physics, Forschungszentrum Jülich, Germany.

0370-2693
http://dx.doi.org/10.1016/j.physletb.2012.05.066

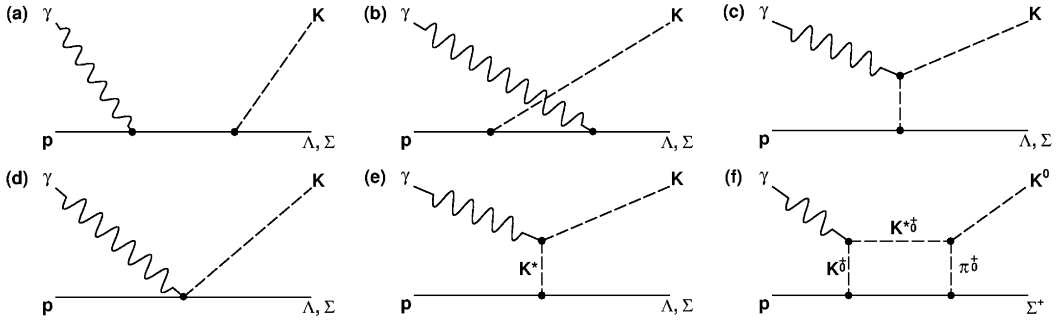

Fig. 1. Diagrams contributing to charged and uncharged kaon photoproduction. The Born diagrams are shown in (a)–(d). Non-strange resonances may contribute as intermediate states in the s-channel (a) and u-channel (b). The t-channel meson exchange (c) and the seagull term (d) are proportional to the meson charge, hence contribute only to the charged kaon channel. Vector meson exchange (e) is allowed also for K^0 photoproduction. Diagram (f) visualises subthreshold K^* production with subsequent coupling into the $K^0\Sigma^+$ channel through neutral or charged π rescattering, as explained in the text.

is controversially seen also in lattice QCD calculations [6,7], but correctly reproduced in models which assign an essential role for baryon dynamics to meson fields [8,9]. Such meson–baryon interactions are expected to dynamically generate quasi-bound states in the vicinity of thresholds [10–18].

Meson photoproduction provides a sensitive tool to investigate nucleon excitations. In the experiment presented here the reaction $\gamma p \to K^0\Sigma^+$ was studied from threshold ($E_\gamma = 1047.6$ MeV) to a photon energy of $E_\gamma = 2250$ MeV, i.e. across the K^* production threshold at $E_\gamma = 1678.2$ MeV for the $K^{*+}\Lambda$ final state, and at $E_\gamma = 1848.1$ MeV for $K^{*0}\Sigma^+$. Compared to charged K photoproduction, which has been extensively studied during recent years [19], the K^0 channel has tended to be sidelined. This appears entirely unjustified, though. To study s-channel resonance excitations (Fig. 1(a)), the photoproduction of neutral kaons offers some advantages over charged ones, because the photons cannot directly couple to the (vanishing) charge of the meson. Hence, the t-channel diagram (c) in Fig. 1 does not contribute to the production process. Since this may become dominant in charged kaon photoproduction, the neutral channel provides a cleaner probe for s-channel excitations. However, t-channel processes are not entirely suppressed in K^0 photoproduction. The photon coupling to the K^0–K^{*0} vertex remains non-zero and renders a t-channel exchange of a K^* meson possible as is visualised in Fig. 1(e). This opens the opportunity to get a hand on explicit meson–baryon dynamics: Should K^*–hyperon dynamics play a significant role, then K^* production via diagrams of the type 1(f) may yield K^0 photoproduction markedly different above and below the K^{*0} threshold, unmasked by the strong charge-dominated t-exchange in K^+ production. These considerations provided the motivation for our study of the $\gamma p \to K^0\Sigma^+$ photoproduction reaction presented here. Previous data of Crystal Barrel [20] and SAPHIR [21] agree rather well in general, however differences show up just in the energy region of the K^* threshold, prohibiting any clear conclusions on K^*–hyperon dynamics. The goal of the present experiment was to improve this unsatisfactory situation.

2. Experiment

The experiment was performed at the tagged photon beam of ELSA, produced from an electron beam of $E_0 = 3.2$ GeV, using the combined Crystal Barrel and TAPS detector setup which is described in detail in Ref. [22]. In the present experiment we used an unpolarised beam by azimuthal averaging over coherent bremsstrahlung peaks from a 500 µm thick diamond crystal, which were subsequently set at 1305, 1515 and 1814 MeV. Contained in a 5.3 cm long cryogenic cell with 80 µm Kapton windows, liquid hydrogen served as target material. The tagging system was run at electron rates up to 10^7 Hz. In contrast to a previous measurement [20] which was normalised to η production in the $3\pi^0$ decay channel, here the absolute photon flux was determined from the tagged electron spectrum in combination with a fast total absorbing $PbWO_4$ detector to measure the energy dependent tagging efficiency.

3. Event selection and data analysis

The Crystal-Barrel/TAPS detector setup is optimised for multi-photon final states. Therefore, the $K^0\Sigma^+$ reaction was studied in the neutral decay modes $K^0 \to \pi^0\pi^0$ (B.R. 31.4%) and $\Sigma^+ \to p\pi^0$ (B.R. 51.6%), which in total yields 6 photons along with the proton. Event topologies with 6 or 7 cluster hits in the calorimeters were selected. Charged particles were recognised through their signals in a three-layer scintillating fibre detector inside the barrel [23] or ΔE plastic scintillators in front of the TAPS modules. However, the proton detection efficiency was inhomogeneous over the acceptance, and particularly limited at low momentum. Therefore, proton identification was *not* required in the data selection. Instead, the proton was reconstructed by kinematic fitting in the later analysis. This is possible, because the reaction kinematics are overdetermined even if the proton was completely missed. Different event topologies were treated separately. Two charged particle events were discarded. For a 7 cluster event with one charged particle in the final state the proton assignment was unique. 7 neutral cluster hits were also accepted. In this case, all combinatorial possibilities for the proton assignment were processed. The resulting combinatorial background was largely reduced through kinematic requirements in the further analysis. Assuming that all hits are photons and the proton not detected, 6 neutral cluster hits were accepted as well, and the proton reconstructed as for the other topologies.

The tagged photon energy range extended below the $K^0\Sigma^+$ threshold. However, in the analysis a photon energy $E_\gamma >$ 1047.5 MeV was required to reduce random background. Furthermore, it was requested that 3 pairs of neutral (so-called γ) hits can be found with invariant masses in the range of the π^0, namely 110 MeV $\leqslant M_{\gamma\gamma} \leqslant$ 160 MeV. The reaction $\gamma p \to \eta p \to p6\gamma$ provided the most significant background. It was practically eliminated by requiring the invariant mass of the three identified π^0's to *not* lie within the range 470 MeV $\leqslant M_{3\pi^0} \leqslant$ 620 MeV. This corresponds to a 4-sigma wide anti-cut around the η mass. Finally, neutral background events from the electron beamdump (which was located below the floor in front of the Crystal Barrel

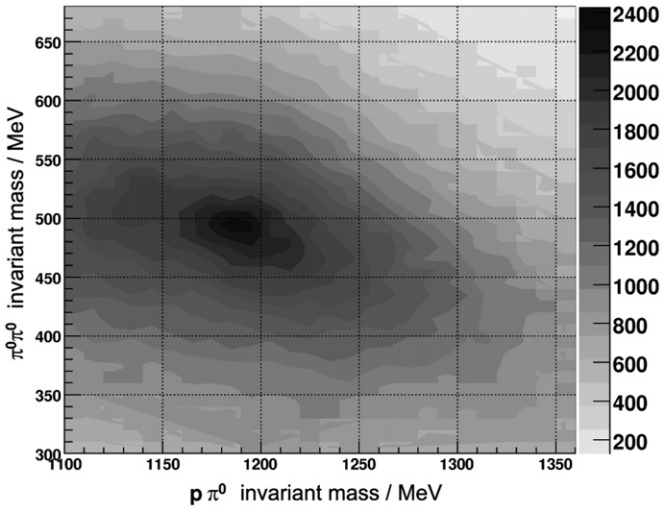

Fig. 2. $\pi^0\pi^0$ against $p\pi^0$ invariant mass distribution after event preselection and kinematic cut, showing a concentration of events in the $K^0\Sigma^+$ final state.

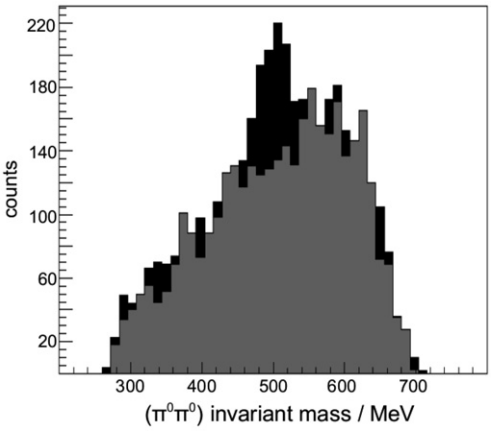

Fig. 3. $\pi^0\pi^0$ invariant mass distribution for the bin 1350–1450 MeV in photon energy and 0–0.33 in $\cos\Theta^K_{\rm cms}$ after a cut on the Σ^+ mass in Fig. 2: 1170 MeV $\leqslant M_{p\pi^0} \leqslant$ 1210 MeV. The grey area represents the simulated background from uncorrelated $3\pi^0$ photoproduction, scaled to the experimental yield outside the signal area (cf. text).

calorimeter) were rejected through their special angular topology.

Based on this preselection, the remaining events were subjected to a kinematic fit to the $\gamma p \to p3\pi^0$ reaction. The photon energy was defined by the tagging spectrometer. Energy and angle parameters for the fit were provided by the final state photon hits. The proton candidate did not enter the fit. In contrast, its momentum vector was determined through the kinematic conditions. With the four components of the proton momentum to be determined and seven conditions (overall energy–momentum and three π^0 masses) the fit still was threefold overdetermined. Σ^+ and K^0 masses were not used as conditions of the kinematic fit. After the kinematic fit an acceptable signal to background ratio was achieved. This is demonstrated in Fig. 2 where the $2\pi^0$ invariant mass is plotted against the $p\pi^0$ invariant mass distribution. A culmination of events is clearly visible around $M_{\pi^0\pi^0} = 490$ and $M_{p\pi^0} = 1190$ MeV, corresponding to the masses of K^0 and Σ^+. As an example, Fig. 3 shows the $\pi^0\pi^0$ invariant mass distribution for the bin 1350–1450 MeV in photon energy and 0–0.33 in $\cos\Theta^K_{\rm cms}$, the kaon centre-of-mass angle, after a cut on the Σ^+ mass region in the $p\pi^0$ mass distribution: 1170 MeV $\leqslant M_{p\pi^0} \leqslant$ 1210 MeV. The cut limits were obtained by minimising the related systematic error induced by background subtraction. In Monte Carlo simulations it turns out that the far dominating background is associated with uncorrelated photoproduction of three neutral pions. The simulated background distribution is shown as the hatched area in Fig. 3. The spectra agree very well with the experimental distributions in all bins. The simulated yield is scaled outside the area of the K^0 signal peak.

The photon energy range was divided into 12 bins of ± 50 MeV width, ranging from 1100 to 2200 MeV. Monte Carlo simulations determined the experimental acceptance individually for each of the three selected event topologies. An important benefit of the almost 4π detection system is the practically flat acceptance. This is visualised in Fig. 4.

4. Results and discussion

Based on the absolute normalisation of the photon flux provided by the tagging system, differential cross sections were determined separately for the 6 and 7 hit topologies. Both agree very well and were then combined into the full squares which are shown in Fig. 5. Associated with the data points are the total statistical errors. The combined systematic error is indicated by the grey bars on the abscissa. It has contributions from the photon flux ($\simeq$5%), the cuts applied in the analysis ($\simeq$5–6%), the kinematic fit ($\simeq$5%) and the simulated acceptance ($\simeq$5.6%). The error of the kinematic fit is induced by a cut on the confidence level, which was required to exceed 0.1. All errors associated with cuts were estimated through the variation of the cuts over a wide range. Hence, they may be considered as upper limits. The most probable errors would be significantly smaller. Also, the error in the photon flux affects the extracted absolute cross sections, but, within a given energy bin, it leaves the form of the angular distribution unchanged.

In comparison to our new data, Fig. 5 also shows the results of previous measurements of Crystal Barrel [20] and SAPHIR [21]. While the older data sets agree relatively well in general, there are significant discrepancies in forward directions and, important for the present investigation, in the energy range of the K^* threshold ($E_\gamma = 1750$–1850 MeV bin). These discrepancies could be resolved by our new data. The differential cross sections of a CLAS measurement presented at conferences (not shown in Fig. 5) [24], which detected the charged $K^0 \to \pi^+\pi^-$ decay, agrees well with our new data within the common detector acceptance.

As can be seen from Fig. 5, directly above the $K^0\Sigma^+$ threshold a differential cross section of $\simeq$0.02 μbarn/sr is obtained with flat angular dependence, typical for s-wave production. The cross section rises with increasing photon energy and also develops an increasing forward peaking, suggesting increasing t-channel contributions. This forward peaking is most pronounced in the $E_\gamma = 1700 \pm 50$ MeV bin. In sharp contrast, the next energy bin exhibits an entirely flat distribution again and a drop of the cross section back to $\simeq 0.02$ μbarn/sr. This is at $E_\gamma = 1800$ MeV, i.e. between the thresholds of $K^*\Lambda$ and $K^*\Sigma$ photoproduction. The differential cross section then remains almost flat and practically constant up to the highest measured energies. This suggests that in the K^* threshold region there is a sudden cross over from a t-channel mechanism back to s-channel production of $K^0\Sigma^+$ with increasing photon energy. As is shown in Fig. 6, this effect is strong enough to become clearly visible in the total cross section which, given the full 4π acceptance, is simply obtained by integration of the differential cross sections. Due to the forward peaking of the cross section below the K^* thresholds, the effect is most pronounced in the most forward angular bin, however. Here, the cross section drops by a factor of four in the vicinity of the K^* thresh-

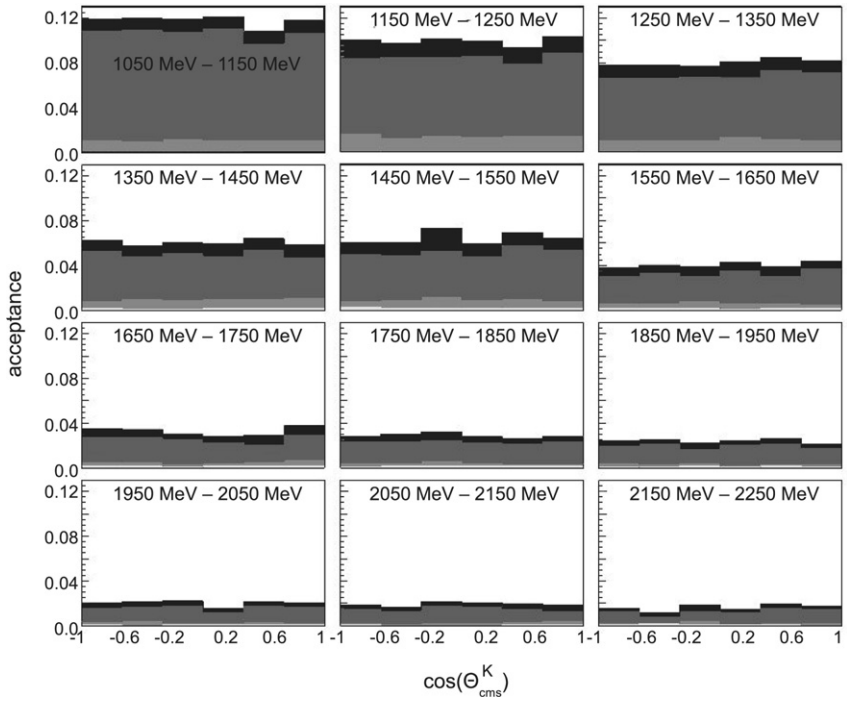

Fig. 4. Simulated acceptance for the $K^0\Sigma^+$ final state. The three event topologies are treated separately: 6 uncharged and 1 charged hits (grey), 7 uncharged hits (white), and 6 uncharged hits (light grey; very small contribution, especially in lowest energy bins). The upper histogram (black) represents the total acceptance.

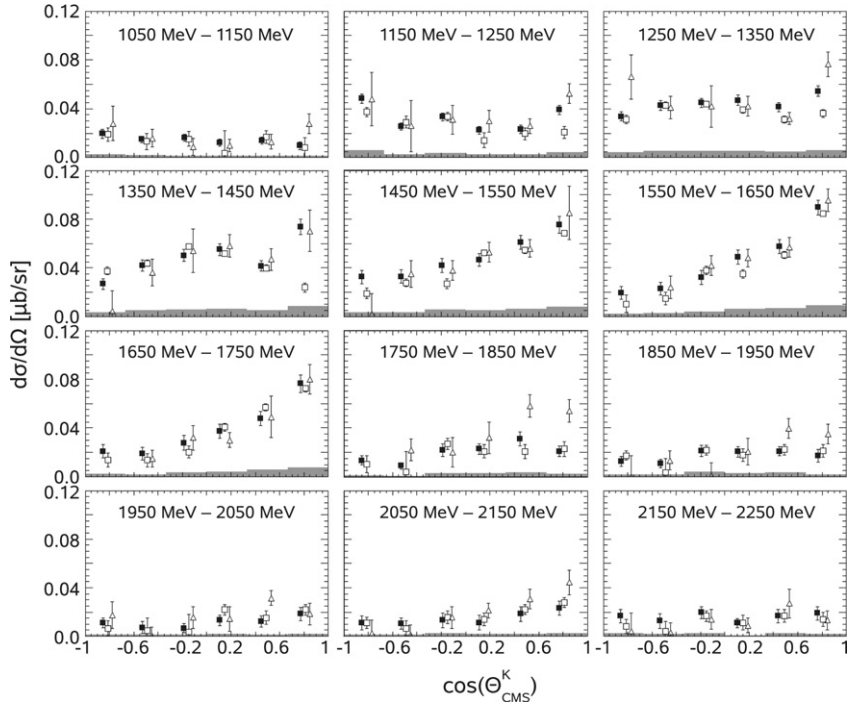

Fig. 5. Measured differential cross sections for $K^0\Sigma^+$ photoproduction as a function of the kaon centre-of-mass angle in ±50 MeV wide bins of photon energy from 1100 to 2200 MeV. The present results (full squares) are compared to previous measurements of Crystal Barrel (open squares) [20] and SAPHIR (triangles) [21]. The error bars are purely statistical. An estimate of the systematic uncertainty is given by the bars on the abscissa (cf. text).

olds, cf. Fig. 7. It remains to be investigated whether a cusp-like structure develops, i.e. a discontinuity[7] in the slope of the cross section.

The structure seems related to a change in the reaction mechanism in the vicinity of the K^* threshold. The role of K^*-exchange was investigated with the K-MAID parameterisation [25], where it is possible to manually change the K^* exchange strength. With standard parameters both, K-MAID and SAID [26], deliver an unsatisfactory description of the data, cf. the dashed and dashed–dotted

[7] Smeared out by the 50.7 MeV width of the K^*.

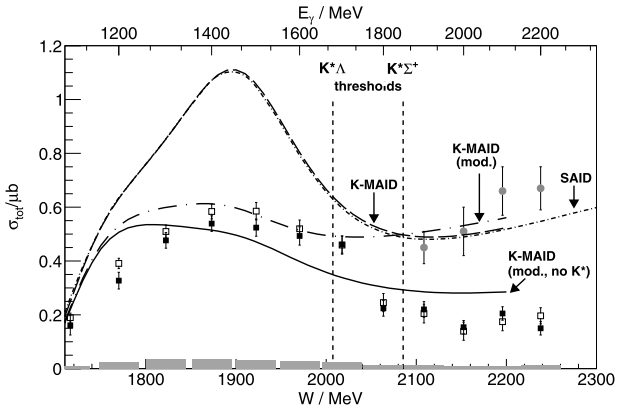

Fig. 6. Total cross section for $K^0\Sigma^+$ photoproduction as a function of the centre-of-mass energy from the present experiment (full squares) in comparison to the previous Crystal Barrel (open squares) [20] data. The vertical lines indicate the $K^*\Lambda$ and $K^*\Sigma^+$ thresholds at $W = 2007.4$ and 2085.5 MeV, respectively. The SAID parameterisation [26] is represented by the short dashed–dotted curve. A K-MAID calculation with standard parameters yields the dashed curve. The long dashed–dotted curve is obtained from K-MAID with the modifications described in the text, and standard K^*-exchange included. The solid curve has the same modifications, but K^*-exchange excluded. Above the K^* threshold the grey circles represent the sum of the $K^0\Sigma^+$ cross section of the present experiment and the $K^{*0}\Sigma^+$ cross section of the work of Nanova et al. [29]. The vertical bars on the abscissa again indicate the systematic error of the present experiment, the errors plotted with the data symbols are purely statistical.

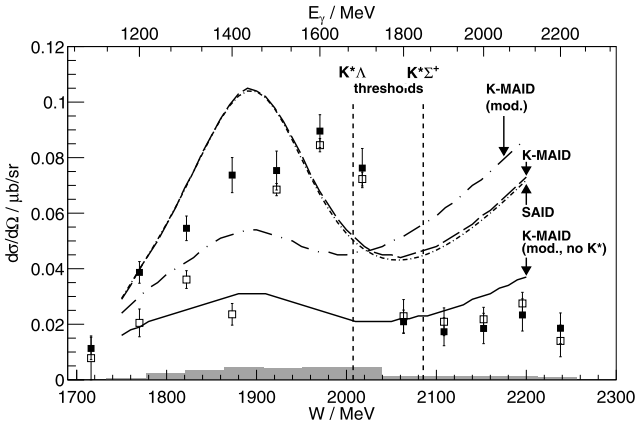

Fig. 7. Cross section for $K^0\Sigma^+$ photoproduction as a function of the centre-of-mass energy from the present (full squares) and a previous (open squares) [20] Crystal Barrel experiment in the most forward angular bin of Fig. 5. Plotted errors and curves represent the same as in Fig. 6, the vertical lines as well.

curves in Fig. 6, respectively.[8] Below the K^* threshold this can be drastically improved by adjusting the couplings of the $S_{31}(1900)$ state to $G_1 = 0.3$ and $G_2 = 0.3$ [25] and reduction of the Born-couplings from 1 to 0.7. Using these modifications we plot two versions of K-MAID in Fig. 6: With standard K^*-exchange (long dashed–dotted curve) and without K^*-exchange (solid curve). As other models [27,28], which were discussed in Ref. [20], neither version is able to reproduce the total cross section in the vicinity of the K^* threshold. The most forward direction (Fig. 7) remains particularly problematic. In general, however, the inclusion of K^*-exchange improves the description of the data below K^* threshold while, in contrast, omission of K^*-exchange renders K-MAID closer to the data above the threshold. At the K^* threshold the K-MAID variants with and without K^*-exchange exhibit a difference of the order of the observed drop, both in the total and the forward differential cross sections.

This leads us to the following speculation. In diagram (e) of Fig. 1 the role of K and K^* may also be interchanged. Of course, no real K^{*0} or K^{*+} is then produced below K^* threshold. However, in the vicinity of the K^* threshold a $K^{*0,+}$ would be produced almost on mass shell. It then strongly couples to a K^0 and a charged or neutral pion. In this way a rescattering diagram of the type 1(f) may in addition contribute to the K^0 channel. Such a contribution will vanish from the K^0 channel once the K^* is produced as a free particle above its reaction threshold, then contributing to the $K^{*0}\Sigma^+$ channel. The strength, which at the dip of the cross section is vanishing from the K^0 channel, should then show up in $K^{*0}\Sigma^+$. In order to test this idea, the measured total cross section of the reaction $\gamma p \to K^{*0}\Sigma^+$ [29] was added to the observed $K^0\Sigma^+$ cross section above the K^* threshold. The result is shown in Fig. 6 as grey circles. Using the sum of the two cross sections, indeed a smooth transition is obtained from below to above the K^* thresholds and the dip structure vanishes.[9]

The loop in Fig. 1(f) could be regarded as a dynamically generated $(K^*\Sigma)^+$ or $(K^*\Lambda)^+$ state in the vicinity of the K^* threshold. Such states are expected in chiral unitary approaches through the interaction of the nonet of vector mesons with the octet of baryons. In Ref. [30] a non-strange isospin 1/2 doublet is indeed predicted at a mass of 1972 MeV, i.e. close to the K^* threshold.

Possible interferences make the role diagram 1(f) non-trivial. Whether it really is able to account for the observed effect can only be decided by detailed calculations which are beyond the scope of this Letter.

Experimentally, the reaction mechanism will be further constrained through polarisation observables. In contrast to a t-channel dominated mechanism, an s-channel intermediate state will provide a genuine spin filter. It is hence expected that, in addition to recoil polarisation and photon asymmetry, in particular the beam–target as well as the beam–recoil asymmetries will shed further light on the mechanism of K^0 photoproduction in the vicinity of the observed dip structure.

The reported structure in the cross section is also close to the $\eta' p$ threshold. In Ref. [31] a significant coupling of vector meson–baryon to pseudoscalar–baryon channels with the same quantum numbers is expected. Consequently, one may speculate that possible K^*–hyperon states may affect the $\eta' p$ cross sections at threshold as well, and thus help to solve the puzzle of $\eta' N$ interactions in both, hadronic and photoinduced reactions [31].

5. Summary and outlook

Using the Crystal-Barrel/TAPS detector setup at the electron accelerator facility ELSA of Bonn University, the reaction $\gamma + p \to K^0 + \Sigma^+$ was investigated from threshold to $E_\gamma = 2250$ MeV. We find an unexpected structure in the differential cross section between the $K^{*0}\Lambda$ and $K^{*0}\Sigma$ thresholds: The angular distribution exhibits a sudden transition from forward peaked to flat with increasing photon energy. In forward directions the cross section drops by a factor of four, generating a pronounced structure even in the total cross section. Detailed calculations will be required to show whether this can be associated with the formation of a K^*–hyperon quasi-bound state. To experimentally shed more light on the threshold structure it will be mandatory to exploit polarisation observables. In particular, the photon beam asymmetry should be sensitive to the parity character of the t-channel contributions, while recoil polarisation and beam–target asymmetry will strongly constrain the quantum numbers of an intermediate s-channel resonance.

[8] The obvious agreement between SAID and K-MAID seems due to the use of K-MAID multipoles in SAID, cf. [26].

[9] This seems somewhat similar to the so-called η-cusp in $\pi^+ n$ photoproduction at the η-threshold, above which the total strength is shared with the ηp channel.

Acknowledgements

Helpful discussions with M. Lutz, E. Oset, A. Rusetsky, Q. Zhao, and L. Tiator are gratefully acknowledged. We thank the staff and shift-students of the ELSA accelerator for their enthusiasm to provide an excellent beam. This work was supported by the federal state of *North-Rhine Westphalia* and the *Deutsche Forschungsgemeinschaft* within the SFB/TR-16. The Basel group acknowledges support from the *Schweizerischer Nationalfonds*.

References

[1] W. Hillert, Eur. Phys. J. A 28 (s01) (2006) 139.
[2] S. Dürr, et al., Science 322 (2008) 1224.
[3] A.J.G. Hey, R.L. Kelly, Phys. Rep. 96 (1983) 71.
[4] S. Capstick, W. Roberts, Prog. Part. Nucl. Phys. 45 (2000) 241.
[5] U. Löring, K. Kretzschmar, B.C. Metsch, H.R. Petry, Eur. Phys. J. A 10 (2001) 309;
U. Löring, B.C. Metsch, H.R. Petry, Eur. Phys. J. A 10 (2001) 395;
U. Löring, B.C. Metsch, H.R. Petry, Eur. Phys. J. A 10 (2001) 447.
[6] N. Mathur, et al., Phys. Lett. B 605 (2005) 137.
[7] Huey-Wen Lin, Chin. J. Phys. 49 (2011) 827.
[8] L.Ya. Glozman, D.O. Riska, Phys. Rep. 268 (1996) 263.
[9] A. Manohar, H. Georgi, Nucl. Phys. B 234 (1984) 189.
[10] R.H. Dalitz, J.G. McGinley, in: E. Ferrari, G. Violini (Eds.), Low and Intermediate Energy Kaon–Nucleon Physics, Reidel, Boston, 1981, p. 381;
R.H. Dalitz, T.C. Wong, G. Rajasekaran, Phys. Rev. 153 (1967) 1617.
[11] P.B. Siegel, W. Weise, Phys. Rev. C 38 (1988) 2221.
[12] N. Kaiser, T. Waas, W. Weise, Nucl. Phys. A 612 (1997) 297.
[13] T. Inoue, E. Oset, M.J. Vicente Vacas, Phys. Rev. C 65 (2002) 035204.
[14] T. Hyodo, S.I. Nam, D. Jido, A. Hosaka, Phys. Rev. C 68 (2003) 018201.
[15] C. Garcia-Recio, M.F.M. Lutz, J. Nieves, Phys. Lett. B 582 (2004) 49.
[16] M.F.M. Lutz, E.E. Kolomeitsev, Phys. Lett. B 585 (2004) 243.
[17] U.-G. Meißner, U. Raha, A. Rusetsky, Eur. Phys. J. C 35 (2004) 349.
[18] B. Borasoy, et al., Eur. Phys. J. A 34 (2007) 161.
[19] R. Bradford, et al., Phys. Rev. C 75 (2007) 035205.
[20] R. Castelijns, et al., Eur. Phys. J. A 35 (2008) 39.
[21] R. Lawall, et al., Eur. Phys. J. A 24 (2005) 275.
[22] D. Elsner, et al., Eur. Phys. J. A 33 (2007) 147.
[23] G. Suft, et al., Nucl. Instrum. Methods A 538 (2005) 416.
[24] B. Carnahan, PhD thesis, Catholic University of America, Washington, DC, 2003; See also F.J. Klein, in: A. Gal, E. Hungerford (Eds.), Proceedings of the Eighth Int. Conference on Hypernuclear and Strange Particle Physics, Newort News, VA, USA, Nucl. Phys. A 754 (2005) 321c.
[25] http://www.kph.uni-mainz.de/MAID/ (version 29.3.2007).
[26] R.A. Arndt, et al., http://gwdac.phys.gwu.edu.
[27] A.V. Anisovitch, et al., Eur. Phys. J. A 25 (2005) 427;
A.V. Sarantsev, et al., Eur. Phys. J. A 25 (2005) 441.
[28] A. Usov, O. Scholten, Phys. Rev. C 72 (2005) 025205.
[29] M. Nanova, et al., Crystal-Barrel/TAPS Collaboration, Eur. Phys. J. A 35 (2008) 333.
[30] E. Oset, A. Ramos, Eur. Phys. J. A 44 (2010) 445.
[31] E. Oset, A. Ramos, Phys. Lett. B 704 (2011) 334.